
Performance prediction of three sides hemispherical dimple roughened solar duct

Vikash Kumar¹, Laljee Prasad^{2,*}

1. Dept. of Mechanical Engineering,
Malla Reddy College of Engineering, Secunderabad 500100, India

2. Dept. of Mechanical Engineering,
NIT Jamshedpur Jharkhand 831014, India
lalprdch1@rediffmail.com

ABSTRACT. *The present paper deals with the results of experimental investigation conducted upon one and three sides concave dimple roughened solar air heater ducts and examine the effects of roughness and flow parameters on thermal efficiency results. The present investigation is carried under the Reynolds number range of 2500-12500, relative roughness pitch of 8-15 and relative roughness height of 0.018-0.045. The augmentation in fluid (air) temperature flowing under three sides concave dimple roughened duct is found to be 34.87% more than one side roughened duct. The plate temperature excess range for three sides roughened duct is significantly lower (12.5-28.5°C) compared to one side roughened duct (17.5-35.5°C). The maximum thermal efficiency is obtained at relative roughness pitch of 12 and relative roughness height of 0.036. The augmentation in thermal efficiency of three sides over those of one side roughened duct is found to be 44-56 % for varying p/e and 39-51 % for varying e/Dh.*

RÉSUMÉ. *Le présent article porte sur les résultats d'une enquête expérimentale menée sur des conduits de chauffage à air solaire de fossette concave et rugueux à une et trois côtés et examine les effets des paramètres de rugosité et d'écoulement sur les résultats d'efficacité thermique. La présente étude est réalisée sous la gamme de nombres de Reynolds de 2500- 12500, la longueur de rugosité relatif de 8-15 et la hauteur de rugosité relative de 0,018-0,045. L'augmentation de la température du fluide (de l'air) s'écoulant sous un conduit de fossette concave à trois côtés est de 34,87% supérieure à celle d'un conduit de fossette à un côté. La gamme de dépassement de la température de la plaque pour un conduit rendu rugueux sur trois côtés est nettement inférieure (12,5 à 28,5 °C) par rapport au conduit rugueux sur un côté (17,5 à 35,5 °C). L'efficacité thermique maximale est obtenue avec une longueur de rugosité relatif de 12 et une hauteur de rugosité relative de 0,036. L'augmentation de l'efficacité thermique de trois côtés par rapport au conduit rugueux à un côté est de 44-56% pour des variations de p/e et de 39-51% pour des variations de e/Dh.*

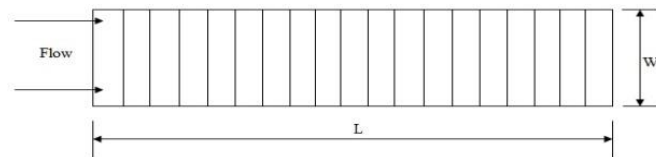
KEYWORDS: *concave dimple, one and three sides roughened duct, relative roughness height relative roughness pitch, solar air heater.*

MOTS-CLÉS: fossette concave, conduit rugueux à un et trois côtés, hauteur de rugosité relative, longueur de rugosité relatif, réchauffeur d'air

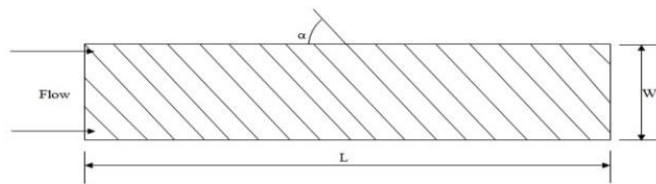
DOI:10.3166/I2M.17.273-293 © 2018 Lavoisier

1. Introduction

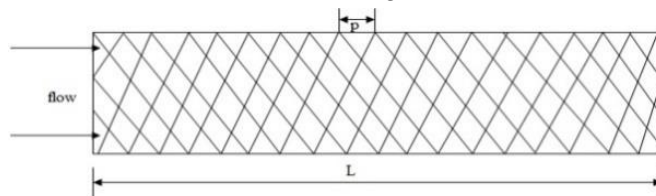
The thermal efficiency of non-roughened flat plate solar collector is low compared to solar water heater due to the fact that convective heat transfer coefficient and thermal capacity of air is low (Gupta *et al.*, 1993; Gupta *et al.*, 1997; Prasad and Saini, 1988). As a result, to that there is the minimum transfer of heat from the collector surface to the under flowing air resulting in higher temperature of the collector. Higher plate temperature leads to higher heat loss to the nearby surroundings (Karwa *et al.*, 2010; Momin *et al.*, 2002). Since last two or three decades, numerous researchers have worked on any method that would result in an appreciable augmentation in the heat transfer rate from the absorber surface to the under flowing fluid (air) (Hans *et al.*, 2010; Hans *et al.*, 2009; Singh *et al.*, 2012; Karwa, 2003). This can be done in multiple ways like increasing the surface area of the collector or by providing artificial roughness on the air flowing side of the collector surface (Saini and Saini, 1997; Alam and Kim, 2017; Saini and Saini, 2008; Sharma and Varun, 2010). Artificial roughness of different geometries under varying geometrical parameters has been used by various researchers that have yielded better results in terms of heat transfer and thermal performance (Karwa *et al.*, 1999; Karwa and Chitoshiya, 2013; Karwa *et al.*, 2001). Figure 1 (a), (b), (c), (d), (e) and (f) show different roughness geometries under varying orientation used by various researchers.



(a) Transverse roughness



(b) Inclined roughness



(c) Expanded metal mesh roughness

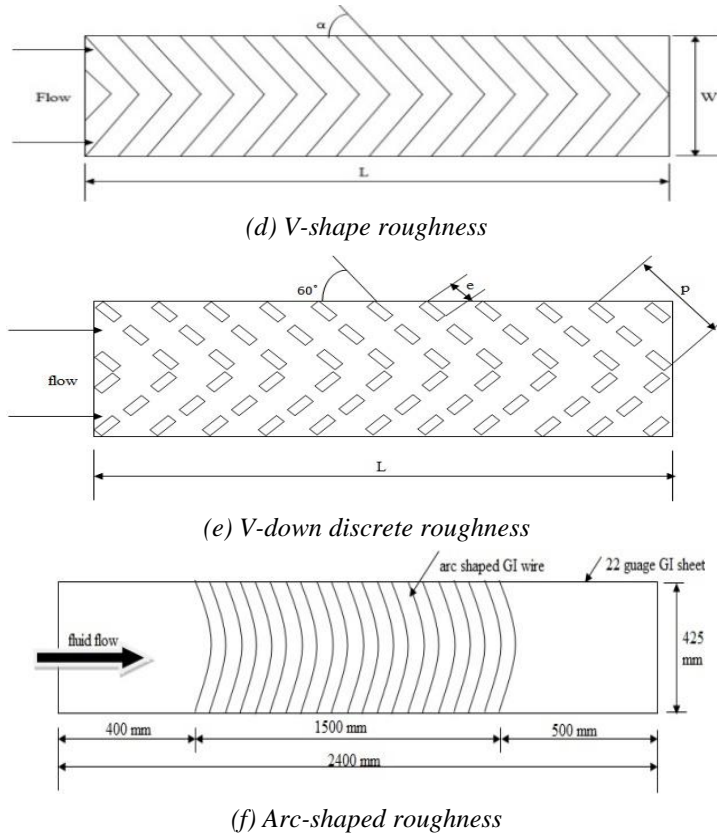


Figure 1. (a), (b), (c), (d), (e) and (f). Various roughness geometries used by researchers

A brief description of different flow pattern due to provision of artificial roughness of different roughness geometries are presented in Figure 2 (a), (b), (c), (d) and (e).

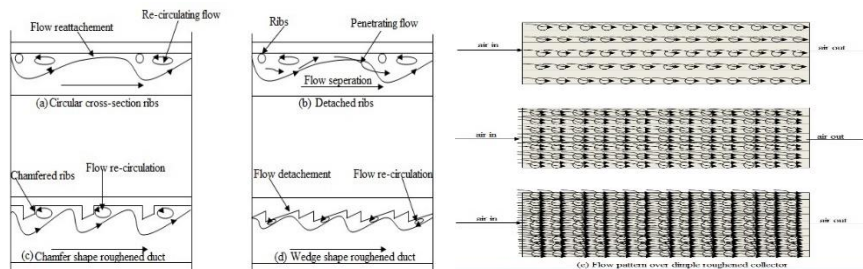


Figure 2. (a), (b), (c), (d) and (e). Flow pattern over different roughness geometries

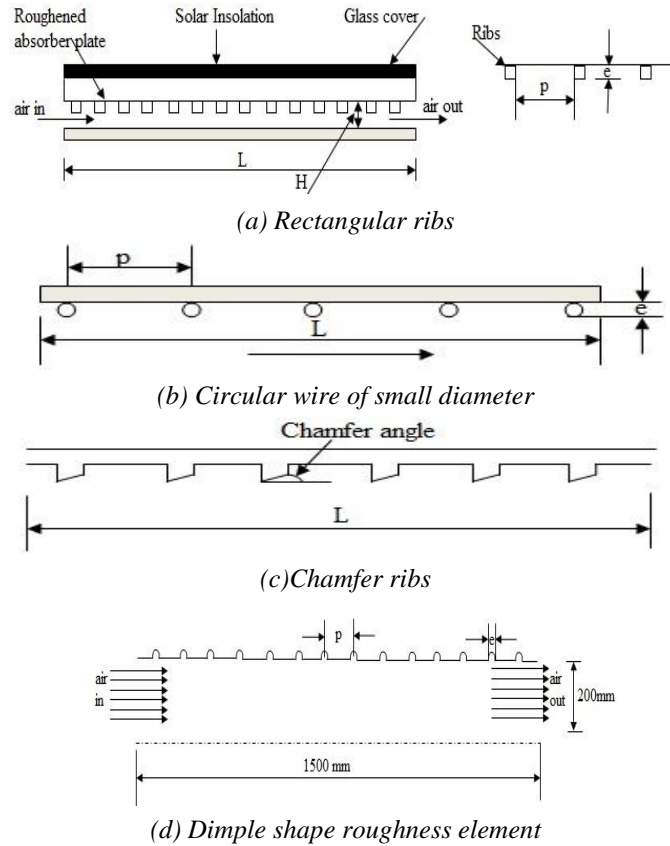


Figure 3. (a), (b), (c) and (d). Orientation of various artificial roughness geometries

For circular cross-section ribs or rectangular wire of small diameter aligned parallel to the flow direction it has been discovered that flow get separated near the ribs and re-adheres in the vicinity of inner rib space at a p/e value of 7 or more (Karwa *et al.*, 2005). The laminar sub-layer lying near to the ribs get destroyed completely at the reattachment point resulting in the enhanced heat transfer coefficient in the vicinity of roughness provided. As soon as the reattachment point is reached, the boundary layer redevelops itself at downstream flow resulting in less heat transfer in the presence of roughened elements (wire or ribs) that extends up to the beginning of next re-attachment point (Prasad and Saini, 1988). For a collector having chamfered ribs aligned positively at relative roughness pitch $p/e \leq 5$, strenuous eddy shedding is observed compared to square or negatively chamfered roughened collector. Reattachment effect in the case of chamfered ribs is seen at p/e as low as 5, thereby reducing the recirculating flow region and laminar sub-layer thickness (Karwa *et al.*, 2010;). The Literature reveals that heat transfer augmentation is more when the roughness element is aligned at inclination or is v-shaped roughened instead of

transverse roughness pattern (Momin *et al.*, 2002). When the ribs are in v-pattern or inclined to the flow, secondary flow (flow of heated secondary air in contact with roughness element) is induced due to the inclination of ribs. The heated air (secondary flow) tends to move towards the side walls in case of inclined ribs. In case of v-up or v-down pattern the heated air move towards the side walls and center of ribs respectively. Thus, the entire absorber plate is exposed to the primary air (axially flowing air) which is at comparatively lower temperature with respect to the secondary air, resulting in more heat transfer from the collector surface to the under flowing air (Hans *et al.*, 2010; Hans *et al.*, 2009; Sinhg *et al.*, 2012). It should be noted here that the temperature along the central axis of the flowing air is higher in the case of v-down roughened collector than v-up rib arrangement. This is due to the fact that secondary flow moving towards the central axis gets intermingled with the axial flow (primary flow) causing additional turbulence resulting in higher heat transfer (Karwa, 2003).

Solar air heater roughened with crossed wires mesh as of Saini and Saini (Saini and Saini, 1997), the dimensionless parameter p/e was varied from 0 to 25, as shown in Figure 1(c). The flow of air under expanded metal mesh was quite complex (Karwa *et al.*, 2010). It was noticed that the heat transfer augmentation was not much for $0 < p/e \leq 7$ due to the fact that flow was dominated by vortex formation. For the plate configuration of $7 < p/e \leq 25$, there is an appreciable increase in heat transfer augmentation because of presence of re-attachment effect and secondary flow (Varun and Singal, 2007).

Artificial roughness applied to the absorber plate may be of rectangular or circular cross-section, dimples or protrusions shape, fins, wedge or chamfered or discrete shape ribs etc. Some of these roughness orientations are shown in Figure 3.

The heat transfer augmentation due to provision of artificial roughness is often followed with the pressure drop enhancement across the duct. Pressure drop enhancement is caused mainly due to increase in frictional resistance offered by the roughened element to the flow. Therefore, it is advisable to go for such a roughness geometry that would result in maximum heat transfer augmentation at the cost of minimum pressure drop (Saini and Verma, 2008). The researchers have not only analyzed the effect of flow and geometrical parameters on heat transfer and friction factor, but have also established a mathematical model and given the correlations for heat transfer and thermal performance for better understanding (Ashrae, 1977). Using these correlations, optimal conditions were defined for artificially roughened solar heater, which would give better performance under minimum loss for a given flow and geometrical conditions. (Prasad *et al.*, 2015) carried out investigations on three sides artificially roughened solar air heater and concluded that roughness Reynolds number always corresponds

$$e^+_{opt} = \frac{e}{D_h} \sqrt{\frac{f_r}{2}} \cdot Re = 23$$

to the optimal thermohydraulic performance under varying set of values for p/e , e/D_h

and Re used separately or combined. (Karwa *et al.*, 1999; Karwaw and Chitoshiya, 2013; Karwa *et al.*, 2001; Karwa *et al.*, 2005) carried out investigations on one side roughened ducts with various types of v-shaped roughness geometry. Under equal pumping power criteria for comparison of thermohydraulic performance it was concluded that at lesser values of the Reynolds number corresponding to lesser rate of flow per unit area of the collector, the v-down discrete rib roughened solar duct having relative roughness height e/D_h of 0.06 was best in performance in terms of heat transfer and thermal and thermohydraulic performance among all other roughness geometries (Bhushan and Singh, 2012; Bhagoria *et al.*, 2002; Garg and Prakash, 2000; Hollands and Shewen, 1981).

It is clearly depicted in the literature of artificially roughened solar air heater that most of the roughness provided is in the form of wire, ribs, wire mesh, expanded metal mesh, fins, etc. (Kumar and Prasad, 2017). All these roughness geometries would require a complex manufacturing process and also contributes to the extra weight of the absorber plate. A detailed study of various roughness geometries used by various researchers was given by (Varun *et al.*, 2007). Providing roughness in the form of dimples is considered as enticing roughness geometry as it is easy to fabricate, especially if dimples to be formed are of spherical indentation concave in nature. Dimples do not add any unwanted weight to the absorber plate and can be fabricated using a simpler manufacturing process than those of other roughness element either soldered/welded on the absorber plates (Saini and Verma, 2008).

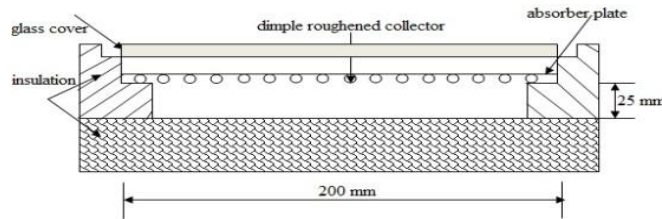
Heat transfer enhancement under the provision artificial roughness has been limited to only one side of the absorber plate (roughened top side) while the bottom and side walls do not participate in heat transfer process. If roughness is provided to the side walls (2 nos) as well, they can participate in the heat transfer augmentation process accompanied by the slightest increase in pressure drop resulting in an appreciable enhancement in heat transfer (Kumar *et al.*, 2018; Kumar and Prasad, 2017; Kumar and Prasad, 2017).

Keeping in mind the above works the present investigation is based on three sides roughened solar air heaters embossed with concave dimples of varying height and pitch as roughness on the flow sides (top and sides) simultaneously on one side dimple roughened solar air heater with the following objectives:

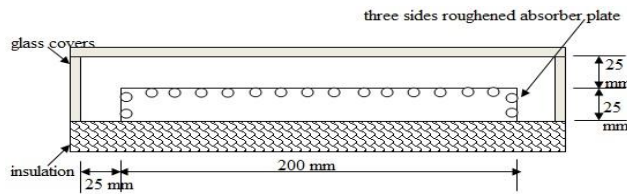
- (1). To develop such solar air heater and carry out experiments under actual outdoor conditions and collect various sets of data for one side as well as three sides roughened ducts.
- (2). To reduce the experimental data to work out for the results in such solar air heaters and validate them with recorded data.
- (3). To discuss the effects of roughness and flow parameters on thermal performance of such solar air heaters.

2. Experimentation and methodology

The test setup used for experimentation in the present work has been fabricated as per the guidelines of ASHRAE Standard 93-77 (1977) for testing roughened solar collectors under actual outdoor conditions using open loop system (Ashrae, 1977). Figure 4 (a), (b), (c) and (d) depict the layout of the experimental setup developed with quality plywood and wooden boards. The setup is accommodated with three ducts parallel to each other, namely a, b and c as shown in figure 5. The present experimental investigations employ the duct a and c containing one side and three sides roughened ducts respectively. Duct b shown in figure 5 accommodate smooth (non-roughened absorber plate) each solar air heater duct setup is 2130mm long, 200mm wide and 50 mm high having 1500 mm as test length and 500 mm as entry length. Only the 1500 mm length is instrumented and the remaining 630 mm entry length serves the purpose of flow stabilization. For one side roughened duct, roughness is provided on the top side serving as absorber plate, two side walls are insulated. 4 mm thick glass cover is on the top side and the bottom is insulated by means of wooden plywood. For three sides roughened duct, roughness is provided to the three sides, i.e. On top and two side walls of the absorber plate. Three sides roughened duct contains three side glass covers and bottom side insulation. The two ducts used in the experimental setup are similar in all terms of dimensions and orientation so that heat transfer and thermal performance characteristics can be directly compared. The absorber plates are painted black to absorb maximum possible incident solar radiation. The set-up is sealed using lightly moistened putty and m-seal to ensure air tight setup. Calibrated copper constantan thermocouples are used to measure the plate temperature. Eighteen numbers of thermocouples are used to measure the plate temperature whose output is given by a digital voltmeter assembled in the setup. Six thermocouples are placed on the top absorber plate of one side roughened duct and rest twelve thermocouples are placed on three sides roughened duct (six on top and six on side walls). Digital thermometers are used to measure the air temperature at six locations along the ducts.



(a) One side roughened plate duct with three sides insulation



(b) Three sides roughened plate duct with one side insulation

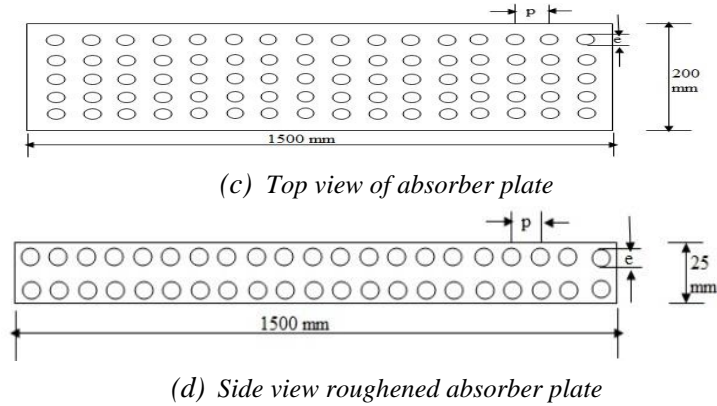
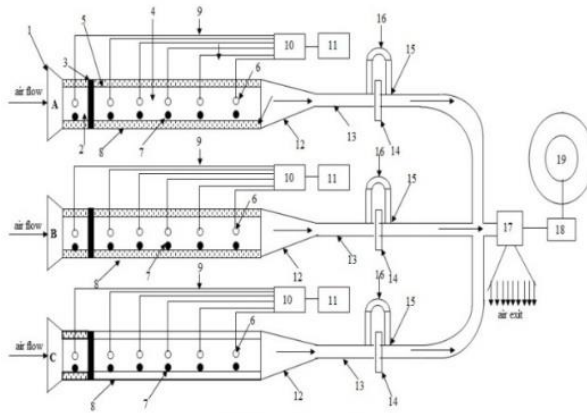


Figure 4. (a), (b), (c) and (d). Schematics of the roughened ducts and the absorber plates

A blower was used to suck the air to flow through the roughened ducts. The desired flow rate of air through the duct was regulated using an auto Variac. Data were taken at intervals of 15 min between 10:00 am to 15:00 pm on clear sky days at six different mass flow rates for each collector simultaneously on various days.



Duct A: One side hemispherical dimple roughened duct; Duct B: Non-roughened (smooth) duct; Duct C: Three sides hemispherical dimple roughened duct

1 Trapezoidal shaped air inlet; 2 Digital voltmeter; 3 Non-roughened duct section; 4 Insulation between entry and test length; 5 Roughened duct section; 6 Insulation; 7 Thermocouple; 8 Thermometer; 9 Glass covers; 10 Copper wire; 11 Selector switch; 12 Diverging section; 13 Cylindrical pipe; 14 Orifice-plate; 15 Flange couplings; 16 U-tube manometer; 17 Blower; 18 Motor; 19 Variac;

Figure 5. Line diagram of the experimental set-up



Figure 6. Typical view of absorber plates



Figure 7. Photograph of the experimental set-up

Table 1. Range of operating parameters

Name of parameter	Symbol	Operating parameter range
Flow rate of air	\dot{m}	(0.0060-0.0250) kg/s
Relative roughness pitch	p/e	8-15
Relative roughness height	e/D _h	0.018-0.045
Ambient temperature	T _∞	(24-44) °C

3. Data reduction

The useful heat gain from the heated absorber plate to the underside flowing fluid (air) can be evaluated using the values air inlet temperature T_i and air outlet temperature T_o. Thus

$$Q_u = \dot{m}C_p (T_o - T_i) \tag{1}$$

where \dot{m} is mass flow rate of air and C_p is the specific heat capacity of air flowing through the roughened duct.

The mass flow rate prevailing through the roughened duct is determined using pressure drop, ΔP_o across the orifice plate:

$$\dot{m} = C_d A_o \left[\frac{2\rho_a \Delta P_o \sin \theta}{1 - \beta^4} \right]^{0.5} \quad (2)$$

The mean temperature of the absorber plate has been calculated based on readings of digital voltmeter that reads the output of thermocouples placed on 'n' different locations of the absorber plate as:

$$T_{pm} = \frac{1}{L} \sum_{i=1}^n T_{pi} \times L_i \quad (3)$$

where, L is test length of collector.

The mean temperature of fluid (air in the present case) is simply the arithmetic mean of air inlet and outlet temperatures and hence calculated as:

$$T_{fm} = \frac{1}{2} (T_i + T_o) \quad (4)$$

D_h = Hydraulic diameter of the duct and is evaluated as:

$$D_h = \frac{4WH}{[2(W + H)]} \quad (5)$$

where, L, H and W are length, height and width of the absorber plate respectively.

The thermal efficiency of artificially roughened solar air heater is defined as the ratio of useful heat gain (Qu) per unit area of the absorber plate to the incident thermal radiation upon it and is calculated as:

$$\eta = \frac{Q_u}{IA_p} \quad (6)$$

where,

Q_u = useful heat gain

I = Incident thermal radiation

A_p = Aperture area of collector

4. Measurement uncertainty

The experimental data recorded during investigation often differ from the actual data due to a lot of unaccountable factors while performing experiments. This deviation of the recorded data from actual data is called as uncertainty. The uncertainty prevailing in the measurement of various parameters has been calculated following a simple procedure suggested by Klein and McClintock (Kline and McClintock, 1953). The procedure for the evaluation of uncertainty has been discussed below:

Let a parameter be calculated using certain measured quantities as,

$$y = y(x_1, x_2, x_3, \dots, x_n)$$

Then uncertainty in measurement of y is given as follows:

$$\delta_y = \left[\left(\frac{\delta_y}{\delta_{x_1}} \delta_{x_1} \right)^2 + \left(\frac{\delta_y}{\delta_{x_2}} \delta_{x_2} \right)^2 + \left(\frac{\delta_y}{\delta_{x_3}} \delta_{x_3} \right)^2 + \dots + \left(\frac{\delta_y}{\delta_{x_n}} \delta_{x_n} \right)^2 \right]^{0.5} \tag{7}$$

Where $\delta_{x_1}, \delta_{x_2}, \delta_{x_3}, \dots, \delta_{x_n}$ are the possible errors in measurements of $x_1, x_2, x_3 \dots x_n$.

δ_y is absolute uncertainty and $\frac{\delta_y}{y}$ is relative uncertainty.

Uncertainty in the measurement of various parameters:

(1). Area of flow, plate and orifice meter

$$\frac{\delta A_p}{A_p} = \left[\left(\frac{\delta L}{L} \right)^2 + \left(\frac{\delta W}{W} \right)^2 \right]^{0.5} \tag{8}$$

$$\frac{\delta A_{flow}}{A_{flow}} = \left[\left(\frac{\delta H}{H} \right)^2 + \left(\frac{\delta W}{W} \right)^2 \right]^{0.5} \tag{9}$$

$$\frac{\delta A_o}{A_o} = \left[\left(\frac{\pi D_o \times \delta D_o}{2} \right)^2 \right]^{0.5} \tag{10}$$

$$\frac{\delta A_o}{A_o} = \left[\frac{\pi D_o^2}{4} \right]^{0.5}$$

(2). Hydraulic diameter

$$\frac{\delta D_h}{D_h} = \frac{\left[\left(\frac{\delta D_h \delta W}{W} \right)^2 + \left(\frac{\delta D_h \delta H}{H} \right)^2 \right]^{0.5}}{\left[2(W \times H)(W + H) \right]^{-1}} \tag{11}$$

(3). Density

$$\frac{\delta \rho_a}{\rho_a} = \left[\left(\frac{\delta P_a}{P_a} \right)^2 + \left(\frac{\delta T_o}{T_o} \right)^2 \right]^{0.5} \quad (12)$$

(4). Mass flow rate

$$\frac{\delta \dot{m}}{\dot{m}} = \left[\left(\frac{\delta C_d}{C_d} \right)^2 + \left(\frac{\delta A_o}{A_o} \right)^2 + \left(\frac{\delta \rho_a}{\rho_a} \right)^2 + \left(\frac{\delta \Delta P_o}{P_o} \right)^2 \right]^{0.5} \quad (13)$$

(5). Useful heat gain

$$\frac{\delta Q_u}{Q_u} = \left[\left(\frac{\delta \dot{m}}{\dot{m}} \right)^2 + \left(\frac{\delta C_p}{C_p} \right)^2 + \left(\frac{\delta \Delta T}{\Delta T} \right)^2 \right]^{0.5} \quad (14)$$

(6). Thermal Efficiency

$$\frac{\delta \eta_{th}}{\eta_{th}} = \left[\left(\frac{\delta Q_u}{Q_u} \right)^2 + \left(\frac{\delta I}{I} \right)^2 + \left(\frac{\delta A_p}{A_p} \right)^2 \right]^{0.5} \quad (15)$$

The uncertainty analysis has been carried out for the entire set of parameter investigated within the operating range and the uncertainty variation of various parameters obtained is presented in Table 2.

Table 2. Uncertainty range in measurement of operating parameter

S. No	Operating parameters	Uncertainty range (%)
1.	Mass flow rate of air	1.43-2.76
2.	Useful heat gain by air	1.85-3.10
3.	Thermal performance	2.57-4.20

5. Results and discussions

Rigorous experimental work has been performed and data for both three sides and one side roughened ducts have been recorded simultaneously at different mass flow rates. Data has been collected for six varying mass flow rates for each duct with specific roughness elements. Altogether 13 different sets of absorber plates for each of the ducts were tested to measure pressure drop across orifice meter, pressure drop across the duct, temperature along the absorber, air temperature at the inlet and the outlet of the ducts and the intensity of incident solar insolation.

5.1. Variation in ambient conditions

Figure 8 shows the variation of solar radiation intensity (W/m^2) and ambient temperature ($^{\circ}\text{C}$) on a typical day with respect to time during the experimental period from 10:00 am to 15:00 pm. It can be seen that as the day progresses, the intensity of solar radiation increases remarkably up to 12:30 pm after which it decreases. As far as the ambient temperature is concerned, it increases monotonously. Figure 8 shows that the maximum value of solar radiation intensity is 921 W/m^2 and ambient temperature is 42°C on that particular day were recorded respectively at 12:30 pm and 14:15 pm.

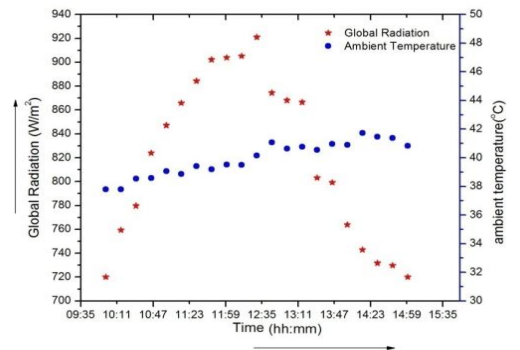


Figure 8. Typical variation of global intensity and ambient temperature with time

5.2. Validation

The present paper is an outcome of experimental investigations conducted upon one and three sides hemispherical dimple roughened solar duct in actual outdoor conditions. Therefore, it is better to validate the three side model using the data obtained from the actual experimentation so as to ensure the exactness of the experimental set-up. The thermal efficiency values for three sides and one side roughened duct were determined using the mathematical model discussed earlier. The present experimental values of thermal efficiency for one side roughened duct was found to be in range and compared well with a similar duct model as of Saini and Verma (Saini and Verma, 2008). Three side dimple roughened solar air heater data is not available for direct comparison. Since one side dimple roughened solar air heater data compare well, therefore, the results for three sides roughened ones are worth to be valid and hence been utilized further. Figure 9 shows the variation of thermal efficiency for both three sides and one side roughened duct from which it can be concluded that three sides roughened duct are far more superior than one side roughened duct in terms of thermal performance. The percentage mean deviation of thermal efficiency for one side roughened duct was found to be $\pm 3.6\%$. The augmentation in the value of thermal efficiency for three sides roughened duct when

compared to one side roughened duct was found to be in the range of 28-41%.

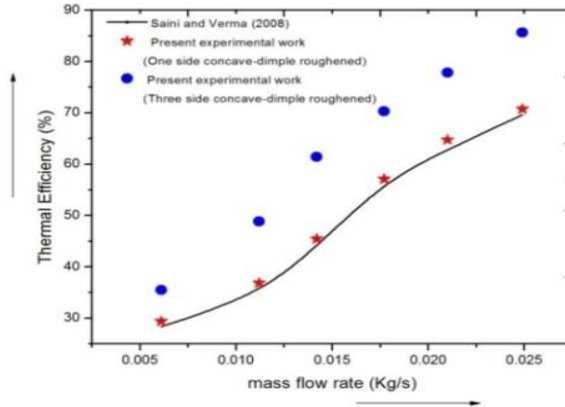


Figure 9. Experimental values of thermal efficiency for one and three sides roughened duct

5.3. Plate and air temperature along test length

Figure 10 shows the variation in air and plate temperature for three sides and one side artificially roughened collector along the test length. As the air travels from inlet to outlet inside these roughened ducts, the destruction of viscous sub-layer due to the provision of artificial roughness in form of hemispherical dimples leads to an enhanced heat transfer from the absorber plate to the under flowing air. Consequently, the plate temperature along the length of the flat plate collector decreases and the temperature of fluid (air) flowing inside these roughened plates increases as a result of convective heat exchange between the absorber plate and air.

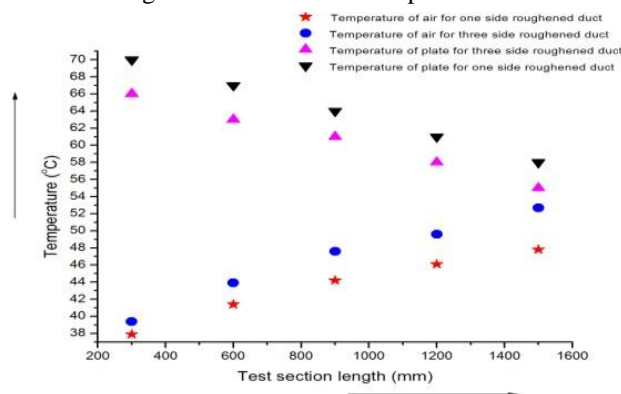


Figure 10. Variation in plate temperature along test length

The same has been shown in Figure 10 from which it can be clearly seen that along the length of the flat plate collector (300 mm to 1500 mm), the rise in fluid temperature for three sides roughened duct is more than the temperature rise for one side roughened duct along the test length of the collector. Meanwhile, for plate temperature, one side roughened duct experiences more temperature rise than three sides roughened duct due to minimal heat transfer to the under flowing fluid (air) along the test length of the collector.

5.4. Plate excess temperature for one and three sides roughened ducts

The mass flow rate has a huge impact on the thermal performance of artificially roughened solar air heater. Figure 11 and 12 shows the plate temperature excess for one side and three sides roughened duct respectively. The plate temperature excess (difference between plate mean temperature and ambient temperature) of both three sides and one side roughened duct decreases with an increase in flow rate. This is attributed to an increase in useful heat gain consequently, reducing plate temperature, which in turn reduces the heat loss from the collector to the surroundings. The effect of increased convective heat transfer coefficient on the plate temperature can be seen in Figure 11 and 12 where the plate temperature excess has been plotted against increasing mass flow rate. The plate temperature excess range for three sides roughened duct is convincingly lower (12.5-28.5°C) than one side roughened duct (17.5-35.5°C). Hence, three sides roughened duct having a higher range of heat transfer operates at lower plate temperatures resulting in higher thermal efficiency due to reduction in heat loss from the absorber plate surface to the surroundings.

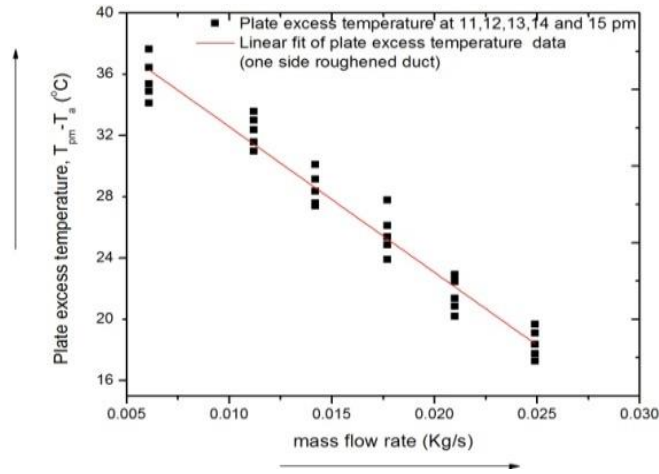


Figure 11. Plate temperature excess vs. \dot{m} (one side roughened duct)

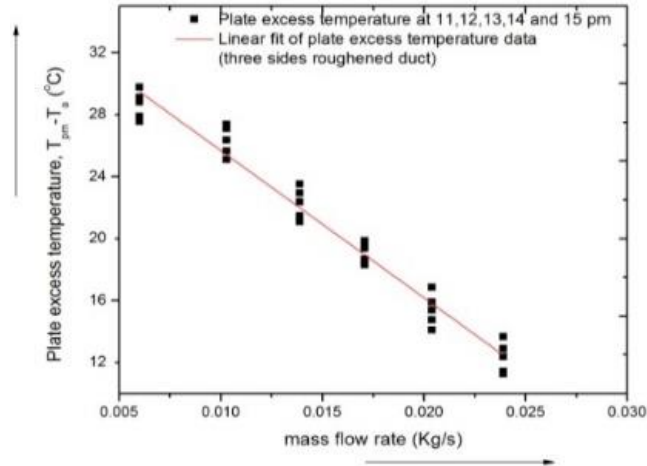


Figure 12. Plate temperature excess vs. \dot{m} (three sides roughened duct)

5.5 Thermal performance

On the basis of the mathematical model employed under present experimental investigations, a comprehensive thermal performance study of concave dimple roughened duct has been carried out for a wide range of flow and geometrical parameters. The results are shown in Figure 13 and 14 as thermal efficiency versus mass flow rate of air. The mass flow rate (\dot{m}) has been varied from 0.0061 kg/s to 0.0249 kg/s. The relative roughness pitch (p/e) has been varied from 8 to 15. The relative roughness height (e/D_h) has been varied from 0.018 to 0.045.

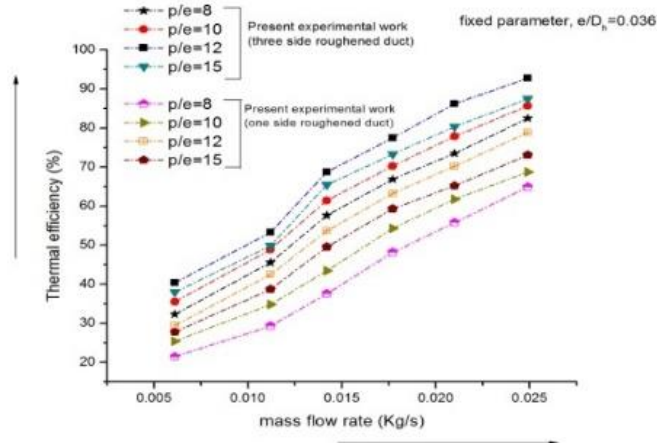


Figure 13. Thermal efficiency vs. Mass flow rate at varying relative roughness pitch

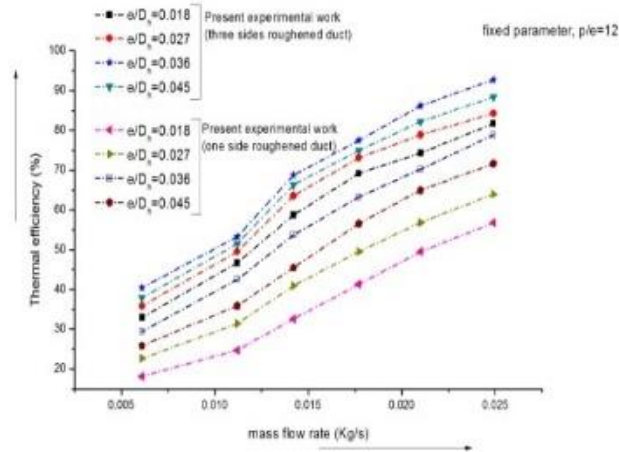


Figure 14. Thermal efficiency vs. Mass flow rate at varying relative roughness height

It can be seen from Figure 13 and 14 that with an increasing mass flow rate, the thermal efficiency of both three sides and one side roughened duct increases. Apart from the top absorber plate, providing roughness to both the side walls of the roughened duct in case of three sides roughened solar air heater enhances the useful heat gain of the under flowing fluid (air) reducing absorber plate temperature that results in reduced heat loss from the roughened surface.

It has been found that for the present geometry provided on the roughened duct, thermal efficiency is maximum corresponding to $p/e=12$ and $e/D_h=0.036$ for both three sides and one side roughened duct. At higher mass flow rates ($\dot{m} > 0.025\text{kg/s}$), there is not much difference between thermal performance of one side and three sides roughened duct. This is due to the fact that at higher mass flow rates, air travels quickly inside the roughened duct and it does not get sufficient time to get affected by the roughness provided inside the duct. The rise in thermal efficiency of three sides over one side roughened duct under varying relative roughness pitch (p/e) is found to be 44-56 % and that of varying relative roughness height (e/D_h) is found to be 39-51 %.

Figure 15 has been drawn to see the maximum enhancement rate of three sides dimple roughened ones over those of one side roughened ones for the range of roughness and flow parameters investigated, which is for p/e value 12 and e/D_h value of 0.036.

Figure 16 has been drawn to see the variation of efficiency ratio i.e. efficiency of three sides over one side ($\frac{\eta_{th3r}}{\eta_{th1r}}$) of the hemispherical dimples roughened solar ducts. The nature was found to be as first increasing then decreasing. This is due to the fact that at mass flow rate $< 0.015\text{ kg/s}$, the air gets sufficient time to be in contact with

the roughness element in case of both one side and three sides roughened solar duct. Due to the destruction of the viscous sub-layer, augmentation in heat exchange phenomena takes place which rises the thermal efficiency of the roughened ducts. But as the mass flow is increased beyond 0.015 kg/s ($\dot{m} > 0.015 \text{ kg/s}$), the air quickly passes over the roughness element without disturbing the viscous sub-layer and hence does not get sufficient time to be in contact with the roughness element consequently hampering the heat exchange phenomena leading to the lesser heat transfer from the plate to the air. As a result, the efficiency ratio first increases then decreases.

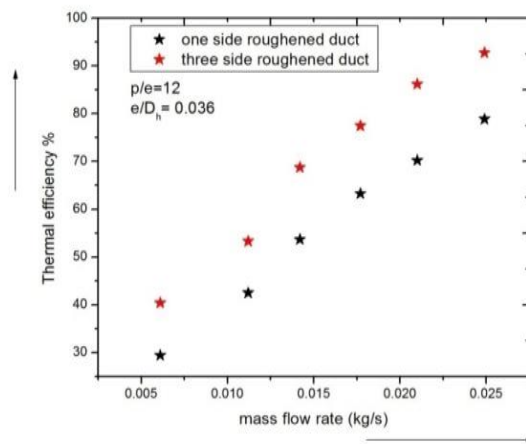


Figure 15. Enhancement in thermal performance

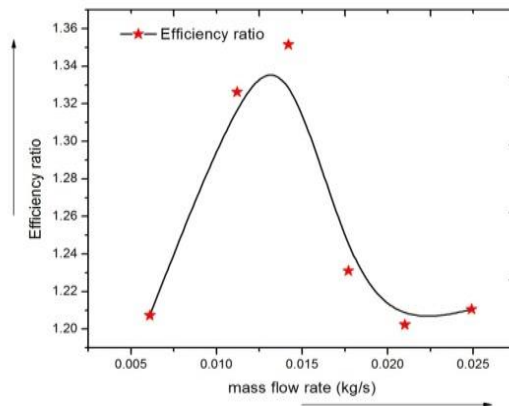


Figure 16. Efficiency ratio vs. mass flow rate

6. Conclusion

The present work is aimed towards determining the rise in thermal efficiency of three sides hemispherical dimple roughened solar duct with respect to similar one side roughened duct under variable flow and operating parameter such as mass flow rate, solar insolation, relative roughness pitch, relative roughness height, etc. A comprehensive experimentation has been performed under actual outdoor condition and the following conclusions can be drawn from the present work:

1. The standard mean deviation in thermal performance of three sides compared to one side roughened duct is ± 3.6 %.
2. The augmentation in fluid temperature for 3-sides compared to 1-side roughened duct is 34.87 %.
3. The abatement of plate temperature in 3-sides compared to 1-side roughened duct is found to be 14.45 %.
4. The plate temperature excess range for three sides roughened duct is significantly lower (12.5-28.5°C) compared to one side roughened duct (17.5-35.5°C).
5. The augmentation is found to be 44-56 % for varying p/e and 39-51 % for varying e/D_h .

The maximum enhancement in efficiency ratio is found to be 1.35 corresponding to $\dot{m}=0.015$ kg/s.

Reference

- Alam T., Kim M. H. (2017). A critical review on artificial roughness provided in rectangular solar air. *Renewable and Sustainable Energy Reviews*, Vol. 69, pp. 387-400. <https://doi.org/10.1016/j.rser.2016.11.192>
- Ashrae S. (1977). Methods of testing to determine the thermal performance of solar collectors. *New York*, pp. 93-77.
- Bhagoria J. L., Saini J. S., Solanki S. C. (2002). Heat transfer coefficient and friction factor correlations for rectangular solar air heater duct having transverse wedge shaped rib roughness on the absorber plate. *Renewable Energy*, Vol. 25, pp. 341-369. [https://doi.org/10.1016/S0960-1481\(01\)00057-X](https://doi.org/10.1016/S0960-1481(01)00057-X)
- Bhushan B., Singh R. (2012). Thermal and thermohydraulic performance of roughened solar air heater having protruded absorber plate. *Int. Journal of Solar Energy*, Vol. 86, No. 11, pp. 3388-3396. <https://doi.org/10.1016/j.solener.2012.09.004>
- Gao W., Lin W., Liu T., Xia C. (2007). Analytical and experimental studies on the thermal performance of cross-corrugated and flat-plate solar air heaters. *Applied Energy*, Vol. 84, pp. 425-441. <https://doi.org/10.1016/j.apenergy.2006.02.005>
- Garg H. P., Prakash J. (2000). Solar energy: Fundamentals and applications. *New Delhi: Tata-McGraw-Hill*.
- Gupta D., Solanki S. C., Saini J. S. (1993). Heat and fluid flow in rectangular solar air heater ducts having transverse rib roughness on absorber plates. *Solar Energy*, Vol. 51, pp. 31-37.

[https://doi.org/10.1016/0038-092X\(93\)90039-Q](https://doi.org/10.1016/0038-092X(93)90039-Q)

Gupta D., Solanki S. C., Saini J. S. (1997). Thermohydraulic performance of solar air heaters with roughened absorber plates. *Sol Energy*, Vol. 61, No. 1, pp. 33-42. [https://doi.org/10.1016/S0038-092X\(97\)00005-4](https://doi.org/10.1016/S0038-092X(97)00005-4)

Hans V. S., Saini R. P., Saini J. S. (2009). Performance of artificially roughened solar air heater- A review. *Renewable and Sustainable Energy Reviews*, Vol. 13, pp. 1854-1869. <https://doi.org/10.1016/j.rser.2009.01.030>

Hans V. S., Saini R. P., Saini J. S. (2010). Heat transfer and friction factor correlations for a solar air heater duct roughened artificially with multiple V-ribs. *Sol Energy*, Vol. 84, pp. 898-911. <https://doi.org/10.1016/j.solener.2010.02.004>

Hollands K. G. T., Shewen E. C. (1981). Optimization of flow passage geometry for air heating, plate-type solar collectors. *Journal of Solar Energy Engineering*, Vol. 103, pp. 323-30. <https://doi.org/10.1115/1.3266260>

<http://www.cwetsolar.com/index.php?option=datos&task=showfilter&estacion=313>

Karwa R. (2003). Experimental studies of augmented heat transfer and friction in asymmetrically heated rectangular ducts with ribs on the heated wall in transverse, inclined, v-continuous and v-discrete pattern. *International-Communications of Heat and Mass Transfer*, Vol. 30, No. 2, pp. 241-250. [https://doi.org/10.1016/S0735-1933\(03\)00035-6](https://doi.org/10.1016/S0735-1933(03)00035-6)

Karwa R., Bairwa R. D. Jain B. P., Karwa N. (2005). Effects of rib angle and discretization on heat transfer and friction in an asymmetrically heated rectangular duct. *Journal of Enhanced Heat Transfer*, Vol. 12, No. 4, pp. 343-355. <https://doi.org/10.1615/JEnhHeatTransf.v12.i4.40>

Karwa R., Chitoshiya G. (2013). Performance study of solar air heater having v-down discrete ribs on absorber plate. *Energy*, Vol. 55, pp. 939-955

Karwa R., Sharma A. and Karwa N. A. (2010). Comparative study of different roughness geometries proposed for solar air heater ducts. *International Review of Mechanical Engineering (IREME). Special Issue on Heat Transfer*, Vol. 4, No. 2, pp. 159-166.

Karwa R., Solanki S. C., Saini J. S. (1999). Heat transfer coefficient and friction factor correlations for the transitional flow regime in rib-roughened rectangular ducts. *International Journal of Heat and Mass Transfer*, Vol. 42, pp. 1597-1615. [https://doi.org/10.1016/S0017-9310\(98\)00252-X](https://doi.org/10.1016/S0017-9310(98)00252-X)

Karwa R., Solanki S. C., Saini J. S. (2001). Thermohydraulic performance of solar air heaters having integral chamfered rib roughness on absorber plates. *Energy*, Vol. 26, pp. 161-176. <https://doi.org/10.1016/j.energy.2013.03.068>

Kline SJ., McClintock FA. (1953). Describing uncertainties in single sample experiments. *Mechanical Engineering*, Vol. 75, pp. 3-8.

Kumar V., Prasad L. (2017). Experimental investigation on heat transfer and fluid flow of air flowing under three sides concave dimple roughened duct. *International Journal of Mechanical Engineering and Technology (IJMET)*, Vol. 8, No. 11, pp. 1083-1094.

Kumar V., Prasad L. (2017). Thermal performance investigation of one and three sides concave dimple roughened solar air heaters. *International Journal of Mechanical Engineering and Technology (IJMET)*, Vol. 8, No. 12, pp. 31-45.

Kumar V., Prasad L. (2018). Performance analysis of three-sides concave dimple shape

- roughened solar air heater. *Sustain. dev. Energy Water Environ. Syst.*, Vol. 6, No. 4, pp. 631-648. <https://doi.org/10.13044/j.sdewes.d6.0211>
- Momin A. M. E., Saini J. S., Solanki S. C. (2002). Heat transfer and friction in solar air heater duct with v-shaped rib roughness on absorber plate. *International Journal of Heat and Mass Transfer*, Vol. 45, pp. 3383-3396. [https://doi.org/10.1016/S0017-9310\(02\)00046-7](https://doi.org/10.1016/S0017-9310(02)00046-7)
- Prasad B. N., Kumar A., Singh K. D. P. (2015). Optimization of thermo hydraulic performance in three sides artificially roughened solar air heaters. *Solar Energy*, Vol. 111, pp. 313-319. <https://doi.org/10.1016/j.solener.2014.10.030>
- Prasad B. N., Saini J. S. (1988). Effect of artificial roughness on heat transfer and friction factor in a solar air heater. *Solar Energy*, Vol. 41, pp. 555-560. [https://doi.org/10.1016/0038-092X\(88\)90058-8](https://doi.org/10.1016/0038-092X(88)90058-8)
- Saini R. P., Saini J. S. (1997). Heat transfer and friction factor correlations for artificially roughened ducts with expanded metal mesh as roughness element. *International Journal of Heat and Mass Transfer*, Vol. 40, pp. 973-86. [https://doi.org/10.1016/0017-9310\(96\)00019-1](https://doi.org/10.1016/0017-9310(96)00019-1)
- Saini R. P., Verma J. (2008). Heat transfer and friction correlations for a duct having dimple shape artificial roughness for solar air heater. *Energy*, Vol. 33, pp. 1277-1287. <https://doi.org/10.1016/j.energy.2008.02.017>
- Saini S. K., Saini R. P. (2008). Development of correlations for Nusselts number and friction factor for solar air heater with roughened duct having arc-shaped wire as artificial roughness. *Solar Energy*, Vol. 82, pp. 1118-1130. <https://doi.org/10.1016/j.solener.2008.05.010>
- Sharma M., Varun. (2010). Performance estimation of artificially roughened solar air heater duct provided with continuous ribs. *Journal of Energy and Environment*, Vol. 1, No. 5, pp. 897-910.
- Singh S., Chander S., Saini J. S. (2012). Investigations on thermo-hydraulic performance due to flow-attack-angle in v-down rib with gap in a rectangular duct of solar air heater. *Applied Energy*, Vol. 97, pp. 907-912. <https://doi.org/10.1016/j.apenergy.2011.11.090>
- Varun-Saini R. P., Singal S. K. (2007). A review on roughness geometry used in solar air heaters. *Solar Energy*, Vol. 81, No. 11, pp. 1340-50. <https://doi.org/10.1016/j.solener.2007.01.017>
- Vinod P. D., Singh S. N. (2017). Thermo-hydraulic performance analysis of jet plate solar air heater under cross flow condition. *International Journal of Heat and Technology*, Vol. 35, No. 1, pp. 603-610. <https://doi.org/10.18280/ijht.350317>

